Available online at www.sciencedirect.com
SCIENCE DIRECT
Journal of Power Sources 158 (2006) 295–302
JOURNAL OF POWER SOURCES
www.elsevier.com/locate/jpowsour

Multi-physics simulations of fuel cells using multi-component modeling

Andrei Smirnov*, Andrew Burt, Ismail Celik

West Virginia University, Morgantown, WV 26506-6106, USA

Received 9 July 2005; received in revised form 1 September 2005; accepted 6 September 2005
Available online 25 October 2005

Abstract

Multi-physics simulations based on multi-component multi-solver modeling approach were performed for high-temperature fuel cells. The developed approach was primarily aimed at the design of complex multi-component engineering systems. It extends the libraries of earlier designed multi-physics system with component classes, which makes it particularly suitable for modeling of fuel cell systems. The C++ based class hierarchy enables simple implementations of different physical models based on general 3D PDE (partial differential equations) solvers, or simplified engineering 1D or 2D models. Simulations of solid-oxide fuel cells were performed using a combined transport solver in multi-species environment. The components included the PEN complex (anode, cathode, electrolyte), air/fuel channels, interconnects, seals and ambient environments. Species concentrations, mass, momentum, energy fluxes, and electric potentials were solved for different components. Models for unsteady fluid dynamics of species, heat transport, electrochemistry and electric currents were combined within different components and interfaced for common variables at the inter-component boundaries. The results include steady and unsteady distributions of temperature, species concentrations, mass fluxes and electric potential inside co-flow and cross-flow fuel cells with different number of channels.

Keywords: Fuel cells; CFD; Multi-physics modeling; Multi-component systems; Object-oriented programming

1. Background

Computer simulations of fuel cells involve complex multi-physics modeling, and earlier work on modeling these systems was faced with the challenge of unifying different solution procedures [1–3]. The complexity of modeling is due to the fact that fuel cells are both multi-physics and multi-component systems. The components of a typical fuel cell are: anode, cathode, electrolyte (PEN complex) as well as interconnect, seal, and air/fuel channels. Different physical processes occur inside each component: electrochemistry (PEN), mass transport (channels), electrical current (PEN, interconnects), heat transfer and associated thermal expansion, etc. In a continuous effort of design optimization these components are arranged in a variety of geometrical designs, such as tubular, planar, hexagonal, and in various air/fuel flow configurations: co-flow, counter flow, cross-flow, as well as mixed configurations. In addition to this, fuel cells arrangements in stacks also present a complex optimization problem.

In the previous work the authors developed a multi-physics approach for modeling a broad class of problems of discrete and continuum dynamics [4], which was implemented in a multi-physics simulation system *MulPhys* (http://www.mulphys.com). This approach is especially suitable for handling segregated or *multi-component* systems, where different physical phenomena occur in different regions of space. A variety of naturally occurring and human-made structures fall into this category, such as biological and geological structures, as well as many engineering systems. In this study the approach was applied to the modeling of fuel cells, which represent typical multi-component multi-physics systems. In modeling these systems it is important to provide a simulation environment capable of incorporating different solution methods and numerical schemes, while enabling their inter-dependence. A distinct feature of a fuel cell system is that some physical processes, such as gas flow and electrical fields, are restricted to certain regions of space, while other, such

* Corresponding author. Tel.: +1 304 2933111; fax: +1 304 2936689.
E-mail address: andrei.v.smirnov@gmail.com (A. Smirnov).

0378-7753/$ – see front matter © 2005 Elsevier B.V. All rights reserved.
doi:10.1016/j.jpowsour.2005.09.012

as heat transfer span multiple regions. Our challenge in designing the simulation system was to incorporate this feature into the modeling paradigm.

2. Method

Earlier simulations of fuel cells performed by the authors [5–7] prompted the introduction of a physical *component* as a new entity of the multi-physics modeling framework [4]. A component is this case represents a well defined region of space governed by one or more physical laws. Fig. 1 shows the UML (Unified Modeling Language) diagram [8] (http://www.uml.org) of the class hierarchy designed for the adequate representation of multi-component systems. In this description the system consists of *domains*, where each domain is a collection of *components*, with each *component* represented by a set of models. Each model is defined by a collection of variables and methods to manipulate them.

In a single processor simulation one domain is usually used to represent one fuel cell, while in a multi-processor case multiple domains are used, with each domain assigned to one processor. In this case one domain can still represent a single fuel cell or a part of it. Multi-processor simulations can be used to model the behavior of stack of fuel cells, or to do a statistical analysis of their performance, such as risk analysis. In the first case a fast inter-processor communication is essential for the efficiency of simulation, and a computer cluster is usually an appropriate implementation medium. In the second case a statistically independent sample is needed, and no inter-processor communication is necessary. A large number of distributed loosely coupled processors, such as provided by an emerging grid-computing environment will be suitable for this purpose.

Following this approach, the setup of a system consists of two parts: geometric design and physical modeling. During geometric design the shape of the domain is created, including all its components. Then each component is discretized into control-volumes or elements. Each element will be automatically assigned a number corresponding to the type of the component it belongs to.

In the stage of physical modeling each model is defined by specifying dependent variables and methods to update them

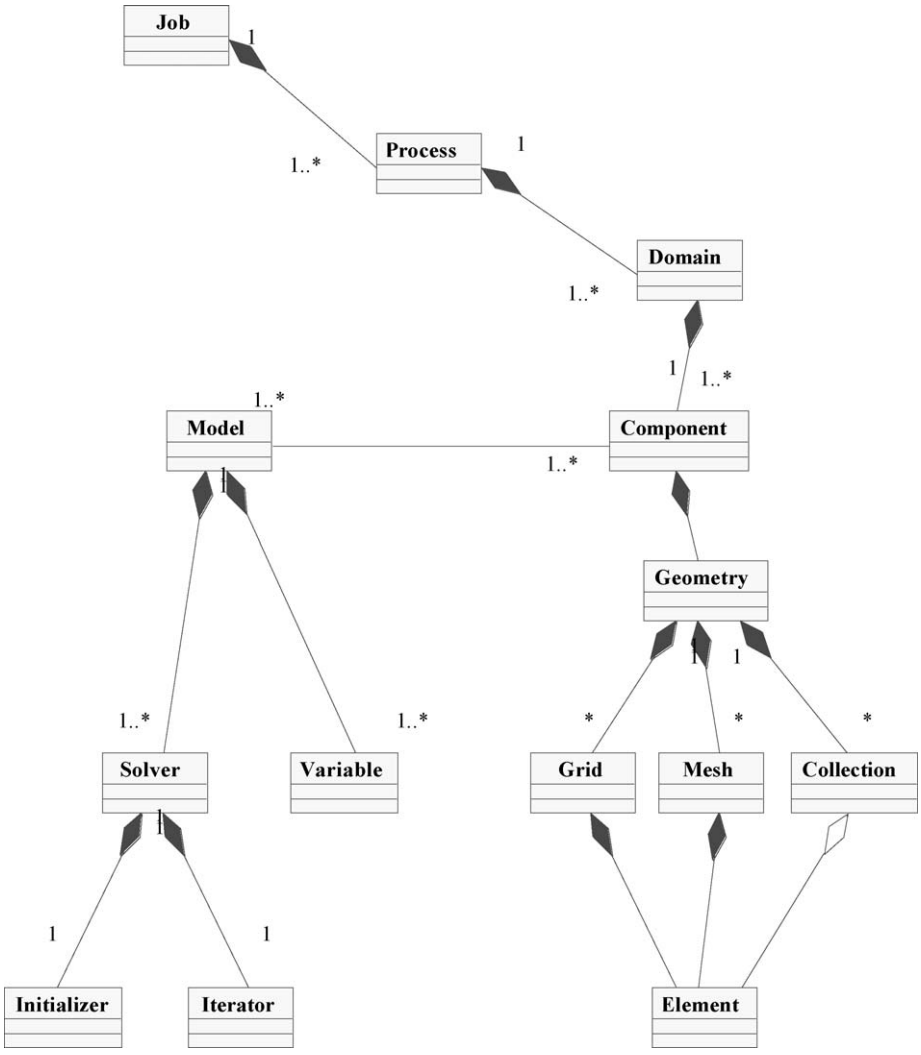

Fig. 1. UML diagram of class hierarchy.

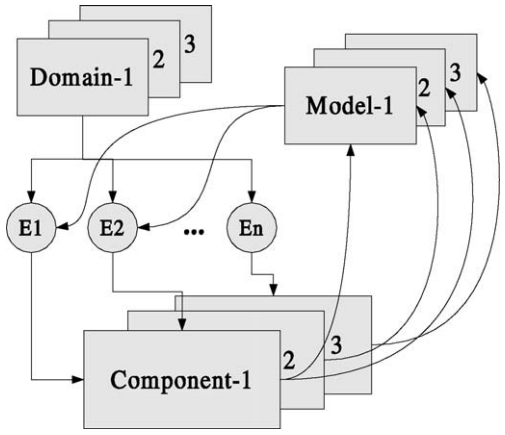

Fig. 2. Design schematics for a multi-physics multi-component system.

(iterators). Models represent physical processes and are not related to any particular geometry or part of a physical space. In the final stage the components are specified, with each component being a simple list of models which belong to it. At this point the geometry is linked to physics by assigning a set of models for each component (Fig. 2). This scheme enables an easy incorporation of complex modeling of multi-physics multi-component systems.

Each model is a member of a model class and is characterized by a set of variables, and two functions: the constructor, or *initializer* and the *iterator*. Within each model there is an access list to the elements which belong to the model can be seen in Fig. 2, this linking elements to models is done indirectly through the components. At the same time there is a direct link from each model to domain elements. This scheme allows one to assign multiple models to each element, thus enabling multiple physics in the same region of space. At the same time, component-based modeling also enables one to restrict some physical processes to specific regions of space. For example, if the heat transfer is occurring in multiple components of the domain, the heat transfer model will have a list of pointers to all the elements of the domain involved in heat transfer. On the other hand, the gas transport model will be present only in components associated with air/fuel channels. The element-to-component links are generated during the geometric design of the system, while the model-to-element lists are automatically created during the call to model initializer function.

Both initializer and iterator can access various geometrical information for each element. This information is either directly stored for each element, or is computed on-the-fly. For example, the dimensionality of the element, it's order, number of faces, and the access list to the vertexes of the element is directly stored in memory for each element. On the other hand, the information on the face-center vectors, face areas, and face normal vectors, etc. can be computed from the stored information. In some applications it may be favorable to change the ratio of stored to computed data for greater efficiency. For example, the face areas and normal vectors can be computed during the initialization stage and stored in memory for the duration of the simulation. At the same time, in the case when the geometry is changing with time these values should be computed on-the-fly.

It should be noted that a general control-volume discretization scheme used in this modeling framework can be used for both detailed differential as well as coarse-grained integral analysis. A differential analysis can involve finite-difference, finite volume or finite element schemes for solving PDEs, while an integral analysis can be based on 1D or 2D engineering approximations and simplified control-volume balance schemes. The latter has an advantage of simplicity and efficiency. For example, the fluid flow in micro-channels, such as those used in fuel cells, can be approximated with a Poiseuille flow solution, instead of resorting to a computationally expensive finite volume or finite element approximations. Similarly, a 2D surface electrochemistry model can be used instead of a more accurate, but more expensive differential solution inside the PEN complex. Such an approach opens a possibility for multi-scale multi-physics modeling in a simplified control-volume framework.

This modeling framework was implemented in C++ language on a Beowulf cluster. The setup and control of the simulations on the cluster was done remotely from a workstation using a Java-based GUI, which provides the features of remote login and monitoring of distributed simulations, and capable of complex geometric design [9–11].

2.1. Mathematical formulation

In the fuel cell modeling scheme four basic sub-models are used: mass transport, species transport, heat transport, and electric current. The mass, momentum, energy and species conservation equations are:

$$\frac{\partial}{\partial t}\int_{\forall}\rho\,\mathrm{d}\forall+\int_{A}\rho(\vec{V}\cdot\vec{n})\,\mathrm{d}A=-\dot{m}_{\mathrm{wall}},$$

$$\frac{\partial}{\partial t}\int_{\forall}\vec{V}\rho\,\mathrm{d}\forall+\int_{A}\vec{V}\rho(\vec{V}\cdot\vec{n})\,\mathrm{d}A=\sum\vec{F},$$

$$\frac{\partial}{\partial t}\int_{\forall}e_{\mathrm{tot}}\rho\,\mathrm{d}\forall+\int_{A}\left(e+\frac{p}{\rho}+\frac{V^2}{2}\right)\rho(\vec{V}\cdot\vec{n})\,\mathrm{d}A=\dot{Q}_{\mathrm{in}},$$

$$\frac{\partial}{\partial t}\int_{\forall}\rho Y_k\,\mathrm{d}\forall+\int_{A}\rho Y_k(\vec{V}\cdot\vec{n})\,\mathrm{d}A=\dot{\omega}_k A_{\mathrm{wall}} \tag{1}$$

where e_{tot} is the total stored energy per unit mass, e is the internal energy per unit mass, and $\dot{Q}_{\mathrm{in}}$ is the net heat flux into the volume. Wall mass and charge fluxes are:

$$\dot{m}_{\mathrm{wall}}=\nu_{\mathrm{wall}}A_{\mathrm{wall}}\rho,\qquad \dot{\omega}_k=\frac{-i_{\mathrm{den}}}{n_k F} \tag{2}$$

where n is the number of electrons per model of reactant k. The PEN and separator plates are considered to be made of solid material, therefore only the energy equation was solved in these regions, which was simplified to:

$$\frac{\partial}{\partial t}\int_{\forall}e_{\mathrm{tot}}\rho\,\mathrm{d}\forall=\dot{Q}_{\mathrm{in}}+\dot{Q}_{\mathrm{gen}}$$

where the radiative and convective heat fluxes through the surface of the control volume, and the thermal energy transported

by mass-flux, are all included in $\dot{Q}_{\text{in}}$, and the heat source, $\dot{Q}_{\text{gen}}$, is obtained from ohmic heating. The heat of entropy generation results in the following expression:

$$\dot{Q}_{\text{in}} = \sum_{A} \dot{Q}_{\text{cond}} + \dot{Q}_{\text{conv}} + \dot{Q}_{\text{rad}} + \dot{Q}_{\text{mass}},$$

$$\dot{Q}_{\text{gen}} = (i_{\text{den}})^2 R - T\Delta s \dot{\omega}_{\text{H}_2}$$

The total entropy change per mode, Δs is obtained from

$$\Delta s = \Delta \bar{s}^o + R_u \ln \frac{r_{\text{R}}}{r_{\text{P}}}$$

where $\Delta \bar{s}^o$ is the molar change in entropy at standard conditions and r_{R} and r_{P} are the reactant and product activities respectively.

$$r_{\text{R}} = \frac{X_{\text{H}_2} P_{\text{anode}}}{P^*} \left(\frac{X_{\text{O}_2} P_{\text{cathode}}}{P^*} \right)^{1/2}, \qquad r_{\text{P}} = \frac{X_{\text{H}_2\text{O}} P_{\text{anode}}}{P^*} \tag{3}$$

Pressure, P is calculated from the ideal gas law:

$$P = \rho R_u T$$

The electrochemistry model is based on the assumption that the overall chemical reaction occurring in the fuel cell is:

$$\text{H}_{2(\text{g})} + \tfrac{1}{2}\text{O}_{2(\text{g})} \Rightarrow \text{H}_2\text{O}_{(\text{g})}$$

Calculation of the cell potential starts with the Nernst equation:

$$E = E^0 + \frac{R_u T}{2F} \left(\ln \left[\frac{[X_{\text{H}_2}][X_{\text{O}_2}]^{1/2}}{[X_{\text{H}_2\text{O}}]} \right] + \frac{1}{2} \ln \frac{P}{P^0} \right)$$

The pressure is assumed to be the same for both the anode and cathode gas channels. The reversible potential at standard state conditions is obtained from the change in the standard Gibbs free energy.

$$E^0 = -\frac{\Delta G^0}{nF}$$

The corrected cell potential, E_{cor}, is obtained by subtracting the ohmic (η_{ohm}), concentration (η_{con}), and activation (η_{act}) losses (i.e. overpotentials) from the ideal Nernst potential, E:

$$E_{\text{cor}} = E - \eta_{\text{ohm}} - \eta_{\text{con}} - \eta_{\text{act}}$$

All overpotentials are related to the current density, and the activation over-potential is defined by an empirical relation represented by a limiting form of the Butler–Volmer equation:

$$\eta_{\text{ohm}} = i_{\text{den}} R_{\text{net}}, \qquad \eta_{\text{con}} = -\frac{R_u T}{nF} \ln \left(1 - \frac{i_{\text{den}}}{i_L} \right),$$

$$\eta_{\text{act}} = \frac{R_u T}{\alpha n F} \ln \left(\frac{i_{\text{den}}}{i_0} \right)$$

The convective heat transfer coefficient, h_{c}, is calculated from the Nusselt number, which is a function of the Reynolds and Prandtl numbers: $h_{\text{c}} = \frac{N_u k}{L}$.

2.2. Numerical discretization

The spatial discretization method used in the solver is based on control-volume techniques, and is applicable to complex geometries. The basic spatial discretization elements are of an arbitrary polyhedral type, which makes them easily adaptable to arbitrary shaped domains, and generally produces better quality meshes than those based on simple tetrahedral or hexahedral types. The geometry input for the solver was generated using a voxel-based graphical user interface developed by the authors [9–11], and specifically designed for describing multi-component structures.

The discretized equation for the total internal energy can be obtained from the energy equation (1):

$$e^{n+1}_{\text{tot},i} = \frac{e^n_{\text{tot},i}\rho^n_i}{\rho^n_i} - \frac{\Delta t}{\rho^n_i \forall_i} \sum_{k=1}^{N_{\text{f}}} e^n_{\text{tot},k} \rho^n_k (\vec{V}^n_k \cdot \vec{n}) A_k + \frac{\Delta t}{\rho^n_i \forall_i} \dot{Q}^n_{\text{in},i} \tag{4}$$

where, the summation is done over all the faces, N_{f}, of a polyhedral cell. After neglecting potential energy, the total internal energy can be found from the absolute enthalpy:

$$e_{\text{tot},i} = e_i + \frac{P}{\rho_i} + \frac{\vec{V}^2}{2} = h_i + \frac{\vec{V}^2}{2}$$

The absolute enthalpy can be found from

$$h(T) = h^0|T_{\text{ref}} + \int_{T_{\text{ref}}}^{T} C_{\text{p}}\, \text{d}T,$$

$$\dot{Q}^n_{\text{in},i} = \dot{Q}^n_{\text{cond},i} + \dot{Q}^n_{\text{conv},i} + \dot{Q}^n_{\text{wall},i} + \dot{Q}^n_{\text{mass},i} + \dot{Q}^n_{s,i},$$

$$\dot{Q}^n_{\text{cond},i} = \sum_{i=0}^{N_{\text{f}}} \frac{2kk_i}{k + k_i} \frac{A_i(T - T_i)}{\Delta x_i},$$

$$\dot{Q}^n_{\text{conv},i} = \sum_{i=0}^{N_{\text{f}}} (\dot{m}_k e_{\text{tot},i} | \dot{m}_i \le 0 + \dot{m}_k e_{\text{tot},k} | \dot{m}_i > 0),$$

$$\dot{Q}^n_{\text{wall},i} = \sum_{i=0}^{N_{\text{f}}} h_c A_k (T_k - T), \qquad \dot{Q}^n_{\text{mass},i} = \dot{m}^n_{\text{wall},i} e^n_{\text{tot},i} \tag{5}$$

Mass fraction for species $s = 1, \ldots, N_s - 1$ is found from species transport equation:

$$Y^{n+1}_{s,i} = \frac{Y^n_{s,i}\rho^n_i \forall_i}{\rho^n_i \forall_i} - \frac{\Delta t}{\rho^n_i \forall_i} \times \left[\sum_{k=1}^{N_{\text{f}}} (Y^n_{s,k} \rho^n_k (\vec{V}^n_k \cdot \vec{n}_k) + \dot{q}^n_{D_s,i,k}) A_k - \dot{\omega}^n_{s,i} M_s A_{\text{wall},i} \right],$$

$$\dot{\omega}^n_{s,i} = \frac{-i^n_{\text{den},i}}{zF} \tag{6}$$

$$\dot{q}^n_{D_s,i,k} = -\rho D_s \frac{Y^n_{s,k} - Y^n_{s,i}}{\Delta x} \tag{7}$$

the mass fraction for species N_s can be found from the definition of mass fraction:

$$Y_{N_s,i}^{n+1} = 1 - \sum_{s=1}^{N_s-1} Y_{s,i}^{n+1}$$

The molecular weight for the mixture is then obtained from:

$$M_i^{n+1} = \frac{1}{\sum_{s=1}^{N_f} (Y_{s,i}^{n+1})/(M_s)}$$

The molar concentration of species, X, can be found from:

$$X_{s,i}^{n+1} = Y_{s,i}^{n+1} \frac{M_i^{n+1}}{M_s}$$

The partial pressures for each species is then obtained from the mole fraction and the total pressure:

$$P_{s,i}^{n+1} = \frac{X^{n+1}}{P_i^{n+1}}$$

The mixture density is obtained from the ideal gas law:

$$\rho_i^{n+1} = \frac{P_i^{n+1}}{R_i^{n+1} T_i^{n+1}}$$

where the gas constant for the mixture can be calculated as:

$$R_i^{n+1} = \frac{R_u}{M_i^{n+1}}$$

The exit velocity can be found from the mass conservation equation:

$$v_{\text{exit},i}^{n+1} = \frac{1}{A_{\text{exit},i}\rho_i^{n+1}} \times \left[\frac{\rho_i^{n+1}\forall_i - \rho_i^n \forall_i}{\Delta t} + \sum_{k=1}^{N_f} \rho_k^n \left(\vec{V}_k^n \cdot \vec{n}_k\right) A_k - \dot{m}_{\text{wall},i}^n \right],$$

$$\dot{m}_{\text{wall},i}^{n+1} = \sum_{s=1}^{N_f} \dot{\omega}_{s,i}^n A_{\text{wall},i} M_s \tag{8}$$

The pressure drop is obtained from the momentum equation:

$$\frac{\Delta P}{\Delta x} = -\frac{\rho_i^{n+1} v_i^{n+1}\forall_i - \rho_i^n v_i^n \forall_i}{\Delta t} - \sum_{k=1}^{N_f} v_k^n \rho_k^n (\vec{V}_k^n \cdot \vec{n}_k) A_k + \frac{C_f}{2}\rho (v_i^n)^2 \tag{9}$$

where the friction coefficient, C_f is the function of the Reynolds number: $C_f = f(R_e)$, $R_e = \rho v d/\mu$.

3. Results and discussion

The most important processes to be included in fuel cell modeling are heat transfer and species transport. These models were implemented on the basis of the discretized energy transport equation (4) and species transport equation (6). The heat transfer scheme was validated on the analytical solutions for constant gradient heat transfer, and the conservation of mass and momentum has been guaranteed through (8) and (9).

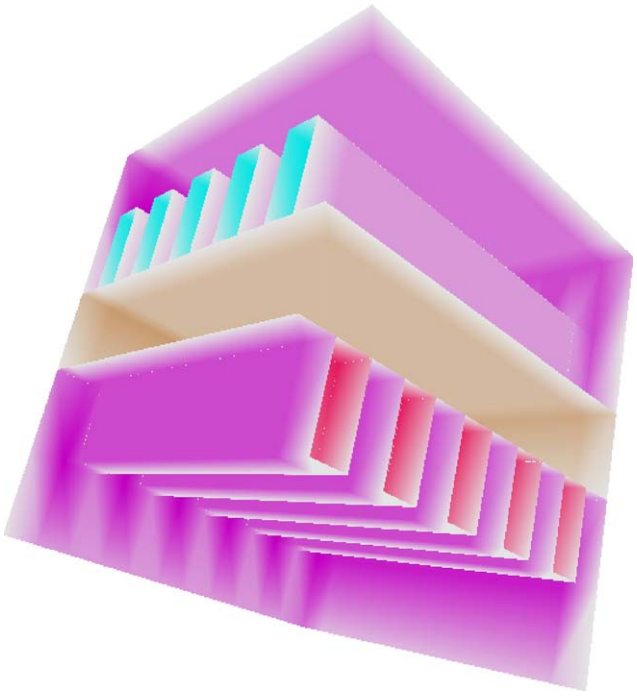

Fig. 3. Geometry of a cross-flow fuel cell.

A planar fuel cell was investigated for two typical flow configurations: co-flow and cross-flow. The geometry of a planar fuel cell consists of a set of straight channels separated by a PEN complex (anode–electrolyte–cathode) and surrounded by seals and interconnects. The 5 air × 5 fuel channel configuration was investigated for both co- and cross-flow cases. Fig. 3 shows a typical cross-flow geometry with 5 × 5 channels, which was produced using a specialized voxel-based GUI [9–11].

A general control-volume discretization employed in this modeling framework was used for a coarse-grained integral analysis of flow, heat, and species transport in various fuel-cell geometries. Fig. 4 shows two cross-sections of the computational grid of 13 × 13 × 7 control volumes for a 5 × 5 co-flow fuel cell. Different components are shown by different colors, which include air/fuel channels, PEN, interconnects, and channel inlet/outlet regions.

Figs. 5 and 6 show the temperature distribution in air and fuel channels of a co-flow fuel cell. The temperature distribution in the PEN of a co-flow fuel cell is shown in Fig. 7. The temperature increase in the direction of the flow is caused by accumulated heat release in the PEN complex and is typical for a co-flow configuration. These figures should be compared to the respective temperature distributions for the PEN (Fig. 8) and air/fuel channels obtained for the cross-flow fuel cell (Figs. 9 and 10). The uneven distribution is due to the localized heat release, which occurs in the areas where both air and fuel channels have a contact through a PEN component. The temperature distribution is also asymmetric with respect to either air or fuel channel axes, which is typical for the cross-flow geometry.

Fig. 11 shows species distribution along the air/fuel channels. As can be seen, even though the fuel is consumed, oxygen

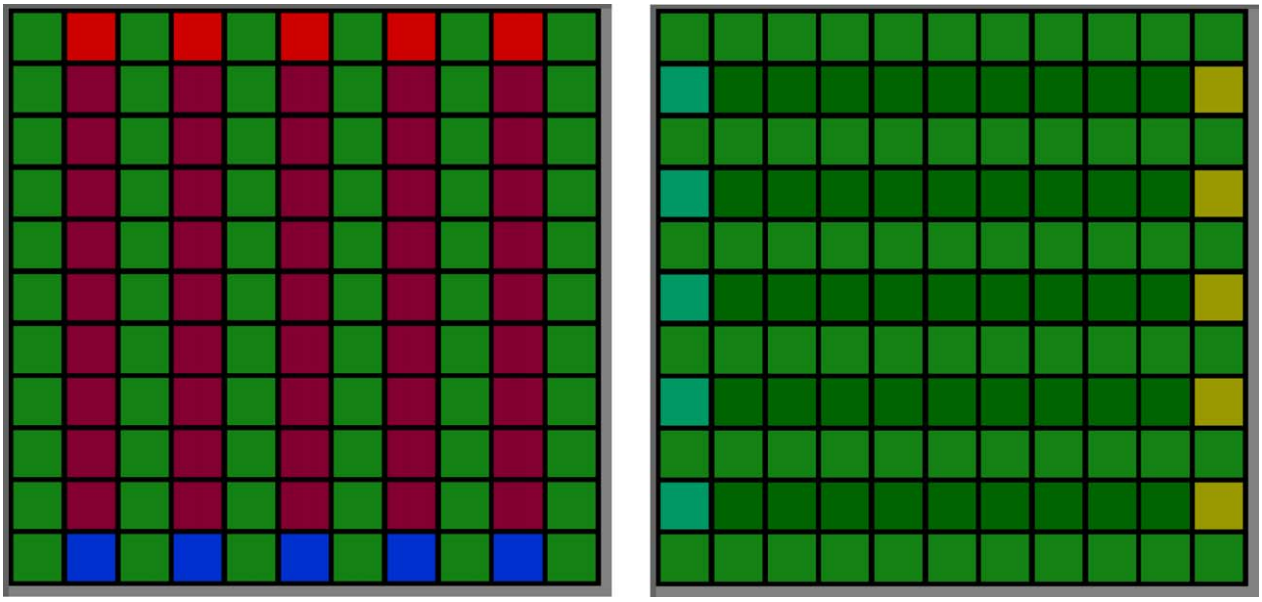

Fig. 4. Cross-sections through a 5 × 5 cross-flow fuel cell.

concentration experiences no appreciable change because of a relatively high mass flow rate in the air channel.

Fig. 12 shows the convergence of the temperature to steady state by considering the variation of three points located in the center of the fuel cell with time. The three points are located in the fuel channel, PEN, and air channel at the center of the five cell cross-flow cell. The thermal response time of the cell is much longer then the response of other phenomena occurring in the cell thus it is used to identify whether the cell has reached steady state.

Temperature and species distributions for different fuel cell configurations are in a qualitative agreement with the behavior of typical fuel cells. In particular, in a previous study, Zitney et al. [12] coupled a FLUENT CFD model with Aspen Plus (a process simulator) to simulate a single channel planar SOFC fuel cell auxiliary power unit. Stevenson et al. [13] and Cheng et al. [14]

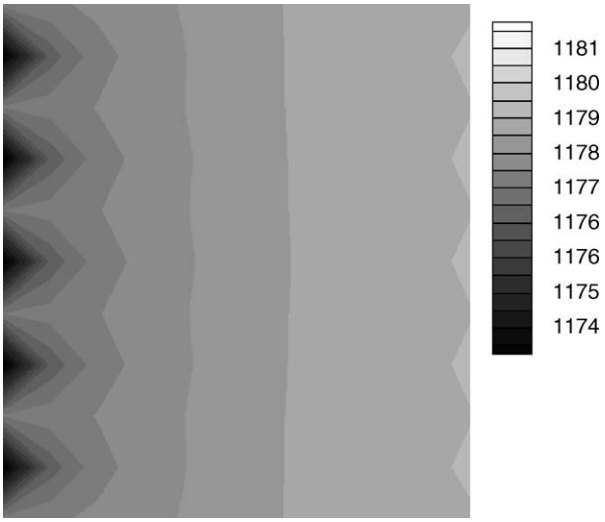

Fig. 5. Temperature (in K) in air channels of a co-flow fuel cell.

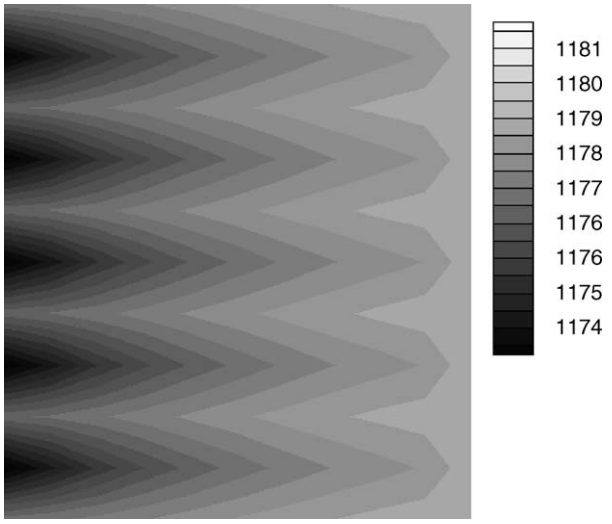

Fig. 6. Temperature in fuel channels of a co-flow fuel cell.

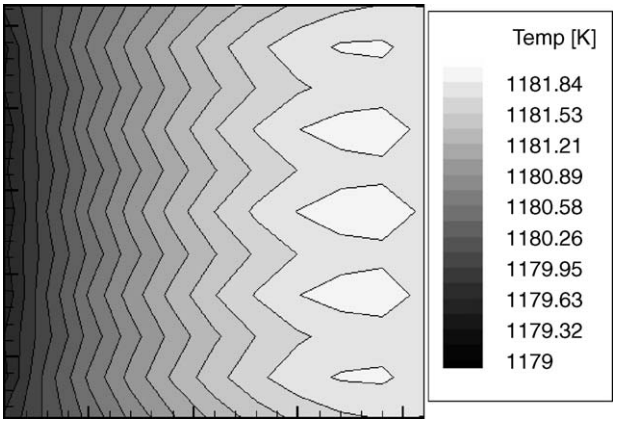

Fig. 7. PEN temperature distribution in a co-flow cell.

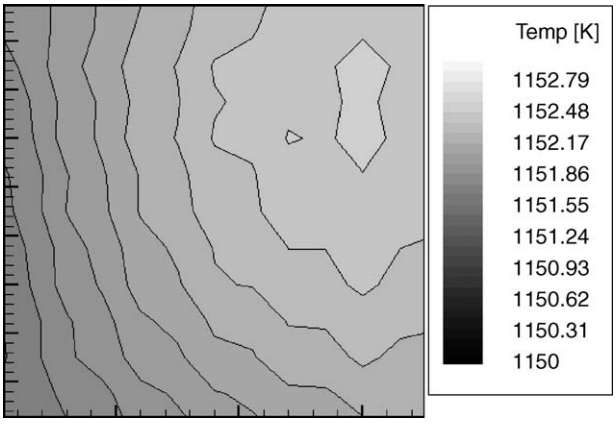

Fig. 8. PEN temperature in a cross-flow cell.

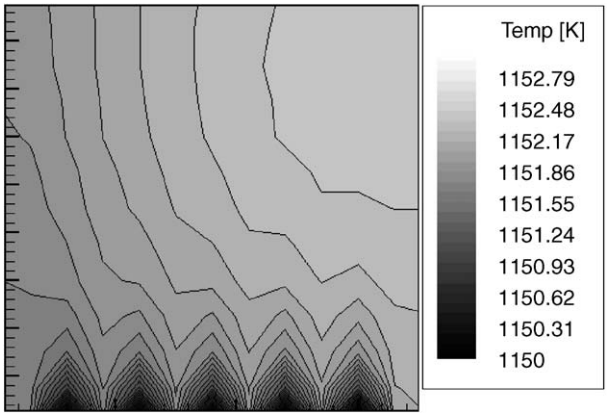

Fig. 9. Temperature distribution in air channels of a cross-flow cell.

conducted similar studies and presented temperature distribution for co-flow, counter-flow, and cross-flow planar SOFC. The results of the last two studies show that the co-flow predicted the most uniform temperature distribution while the cross-flow was the most non-uniform. The cross-flow temperature distributions in all studies had a similar high temperature region located in the corner opposite the air and fuel inlets. Exactly the same trends

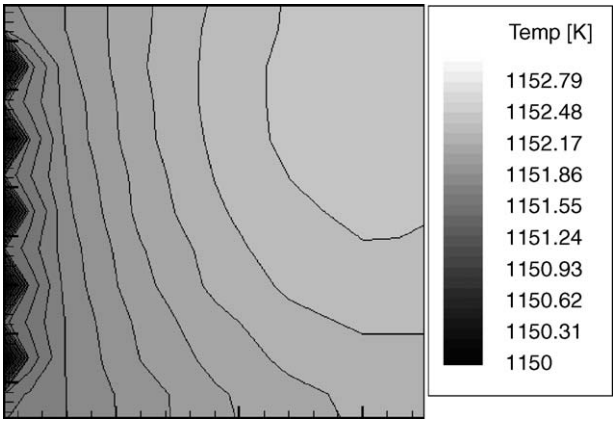

Fig. 10. Temperature distribution in fuel channels of a cross-flow cell.

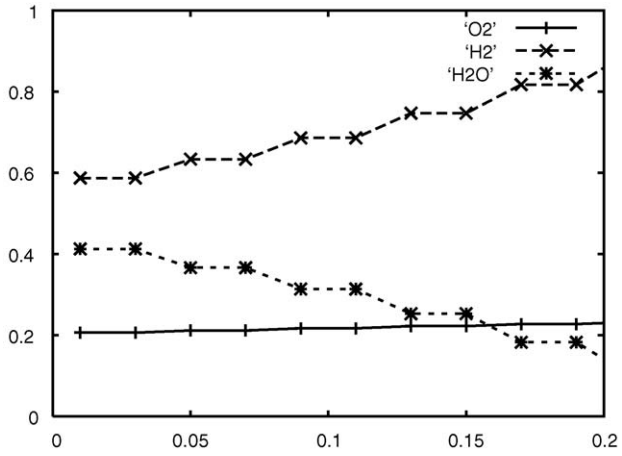

Fig. 11. Species distributions in air/fuel channels.

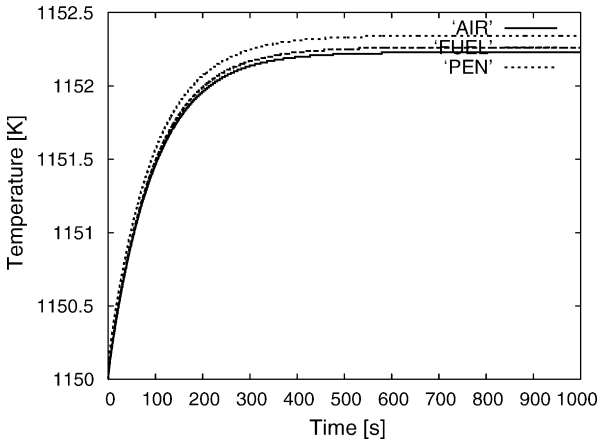

Fig. 12. Transient temperature at three control points.

and the range of temperatures were observed in this study. The temperature distribution in PEN (Fig. 8) also agrees well with the one obtained by Achenbach for a cross-flow fuel cell [1].

The simulations were performed on a Beowulf cluster of 1 GHz, 1 GB computing nodes, with each node of the cluster running a simulation of a single cell. The speed of execution was limited by the process with the minimum time scale (electrochemistry). For the 5×5 channel cross-flow case a convergence to the steady state took about 2000 s of physical time, with a typical time step of 0.01 s, which corresponds to about 30 min of CPU time.

4. Conclusions

A multi-component approach to the modeling of multi-physics systems, such as fuel cells has been proposed and tested on several cases of planar high-temperature fuel cells. Coupled with the appropriate geometrical design tool, the approach enables easy incorporation of various physical models for different regions of space, as well as their co-existence in the same region. In particular, the approach enables coupled solution based on numerical schemes for 3D PDEs, as well as on 1D and 2D engineering approximations. Temperature and species

distributions for different fuel cell configurations are in a good agreement with the earlier studies and is consistent with the behavior of a typical fuel cell.

The approach is general and can be applied to the modeling of other multi-component systems common in science and engineering. For example, biological tissues and geological layers are typical segregated media where the current approach can be effectively used for complex multi-physics modeling.

Parallel implementation of the approach for modeling of fuel cell stacks is straightforward and is the subject of the future work.

Acknowledgments

This work has been sponsored by the Defense Advanced Research Projects Agency under Contract No. W31P4Q-04-C-R219, and by the Parsons Infrastructure & Technology Group, Contract No. 735934-30003-00.

References

[1] J. Achenbach, Three dimentional and time-dependent simulation of a planar solid oxide fuel cell stack, J. Power Sources 49 (1994) 333–348.
[2] J.R. Ferguson, J.M. Fiard, R. Herbin, Three-dimensional numerical simulations for various geometries of solid-oxide fuel cells, J. Power Sources 58 (1996) 109–122.
[3] W. He, Q. Chen, Three-dimensional simulation of a molten carbonate fuel cell stack under transient conditions, J. Power Sources 73 (1998) 182–192.
[4] A.V. Smirnov, Multi-physics modeling environment for continuum and discrete dynamics, Int. J. Modell. Simulat. 24 (3) (2004) 190–197.
[5] A.C. Burt, I.B. Celik, R.S. Gemmen, A.V. Smirnov, A numerical study of cell to cell variations in a SOFC stack, J. Power Sources 126 (1/2) (2004) 76–87.
[6] A.C. Burt, I.B. Celik, R.S. Gemmen, A.V. Smirnov, Cell to cell performance variations within a stack, in: Proceedings of the Eighth International Symposium on Solid Oxide Fuel Cells (SOFC VIII), Paris, France, 2003, pp. 217–223.
[7] A.C. Burt, I.B. Celik, R.S. Gemmen, A.V. Smirnov, Influence of radiative heat transfer on variation of cell voltage within a stack, in: Proceedings of the First International Conference on Fuel Cell Science, Engineering, and Technology, Rochester, NY, 2003, pp. 1487–1500.
[8] J. Rumbaugh, I. Jacobson, G. Booch, The Unified Modeling Language Reference Manual, Addison–Wesley, Reading, MA, 1999.
[9] A.V. Smirnov, H. Zhang, B. Sowers, Voxel-based volume graphics system for multi-physics modeling, in: Proceedings of the Eighth World Multi-Conference on Systemics, Cybernetics and Informatics, vol. 5, Computer Science and Engineering, International Institute of Informatics and Systemics, 2004, pp. 144–149.
[10] A.V. Smirnov, H. Zhang, A. Burt, I. Celik, Fuel-cell simulator interface, J. Power Sources 138 (1/2) (2004) 187–193.
[11] A.V. Smirnov, H. Zhang, A. Burt, I. Celik, Remote interface for geometric design and simulation control, in: H.R. Arabina (Ed.), Proceedings of the 2004 International Conference on Imaging Science, Systems, and Technology: CISST'04, CSREA Press, Las Vegas, NV, 2004, pp. 241–247.
[12] S. Zitney, M. Prinkey, M. Shahnam, W. Rogers, Coupled cfd and process simulation of a fuel cell auxiliary power unit, in: Proceedings of the Second International ASME Conference on Fuel Cell Science, Engineering and Technology, Rochester, NY, 2004, pp. 339–345.
[13] J. Stevenson, S. Baskaran, L. Chick, Y. Chou, J. Deibler, M. Khaleel, O. Marina, K. Meinhardt, D. Paxton, L. Pederson, K. Recknagle, S. Simmer, V. Sprenkle, K. Weil, Z. Yang, P. Singh, G. McVay, Solid oxide fuel cell development at pnnl, in: Proceedings of the ECS International Symposium Solid Oxide Fuel Cells VIII, vol. 2003-07, Paris, France, 2003, pp. 31–39.
[14] C. Cheng, Y. Chang, C. Hong, Multi-scale analysis of transport phenomenon inside the sofc using MD and CFD techniques, in: Proceedings of the Second International ASME Conference on Fuel Cell Science, Engineering and Technology, Rochester, NY, 2004, pp. 347–352.